Geopersia 2026, 16 (1): 129-152
DOI: 10.22059/geope.2025.390516.648809

RESEARCH PAPER

Thermal Effects on Microcracking and Physical Characteristics of Khoramdareh, Natanz, Nehbandan, and Taibad Granites

Saeed Nejati, Mashalah Khamehchiyan *, Mohammad Reza Nikudel

Faculty of Basic Sciences, Tarbiat Modares University, Tehran, Iran

Received: 14 February 2025, Revised: 01 August 2025, Accepted: 08 September 2025

Abstract

This study explores the thermal behavior of four widely used Iranian granites - Khoramdareh, Nehbandan, Natanz, and Taibad - under temperatures ranging from 20°C to 1050°C. The investigation focused on the evolution of microcracks and their impact on key physical properties such as porosity, water absorption, and P-wave velocity in both dry and saturated conditions. Using fluorescence microscopy, linear microcrack density (LMD), microcracks type, and width were analyzed in detail. At 300°C, all granite samples showed an increase in inter-crystalline microcracks, leading to elevated porosity and water absorption. At 600°C, the quartz phase transition at 573°C resulted in volumetric expansion, causing a temporary decrease in porosity and an increase in P wave velocity. For example, the dry P wave velocities at 600°C were 4.77 km/s for Taibad, 4.71 km/s for Khoramdareh, 3.84 km/s for Natanz, and 5.12 km/s for Nehbandan. Above 750°C, trans-crystalline microcracks became dominant, significantly increasing porosity and water absorption while reducing P wave velocity. Nehbandan granite suffered structural failure at 600°C, whereas Natanz exhibited the highest LMD at 750°C, indicating severe internal damage. The study highlights the importance of microcracks evolution and mineralogical transformations, particularly quartz phase transitions, in controlling granite's thermal stability. Three critical thresholds (300°C, 600°C, and 750°C) were identified as turning points in the deterioration process. Additionally, this research introduces a novel methodological approach, combining fluorescence microscopy with physical testing to achieve detailed characterization of thermal damage. By extending the temperature range up to 1050°C, the study provides valuable insights into granite performance in fire-prone and heat-exposed environments.

Keywords: Iranian Granite, Thermal Expansion, P-Wave Velocity, Microcrack Analysis, Fluorescence Thin Section.

Introduction

Temperature variations significantly influence the inherent and physical properties of rocks. Inherent properties, such as mineral composition and microcracks patterns, are unique to each rock and often govern other characteristics, including strength. Understanding the effects of temperature is crucial for predicting rock behavior in various engineering and geological applications. The thermal response of minerals, and consequently rocks, varies considerably. Heat application causes thermal expansion in minerals, but this expansion is not uniform; each mineral has a specific coefficient of thermal expansion determined by its physicochemical conditions and atomic structure.

As temperature increases, particles and ions in the crystal lattice vibrate more intensely, altering atomic or ionic bonds and causing dimensional changes in crystal unit cells. These changes can lead to the expansion or contraction of the rock's volume, a phenomenon known

* Corresponding author e-mail: khamechm@modares.ac.ir

as thermal expansion (Taylor, 1972; Hazen & Finger, 1982). The differing thermal expansion coefficients of granite's constituent minerals result in microcracks with diverse patterns.

For instance, the volumetric thermal expansion coefficients for quartz at 400°C and 800°C are 69×10^{-6} °C^{-1} and -3×10^{-6} °C^{-1}, respectively. In feldspars, these values range from 12 to 27×10^{-6} °C^{-1} at 400°C and 20 to 33×10^{-6} °C^{-1} at 800°C. For hornblende, the coefficients are 28×10^{-6} °C^{-1} at 400°C and 33×10^{-6} °C^{-1} at 800°C (Skinner, 1966). These variations induce compressive or tensile stresses at crystal boundaries: compressive stress forms when a mineral expands more than its neighbor, while tensile stress occurs when it expands less. Such stresses create microscopic microcracks when exceeding the rock's strength threshold (Fredrich & Wong, 1986).

When thermal stresses are significant and materials cannot accommodate strain during rapid cooling, microcracks form due to differences in thermal expansion coefficients (Hale & Shakoor, 2003; Hall, 1999; Hall & Thorn, 2014; Skinner, 1996; Yavuz et al., 2010). Rocks' responses to heat depend on various factors, including mineral composition, petrographic characteristics (e.g., mineral shape, size, and arrangement), and microstructural features like crystal boundaries and porosity (Murru et al., 2018).

Granite's mineralogical composition is pivotal in microcracks initiation and microcracks patterns. Research shows that mineralogical composition influences stress distribution and microcracks development more significantly than thermal expansion alone (Vázquez et al., 2015). Feng et al. (2023) and Zuo et al. (2016) demonstrated that thermal-induced microcracking primarily arises from mismatched thermal deformation among minerals. The expansion caused by temperature rise weakens grain boundaries due to thermodynamic heterogeneity, including differing thermal expansion coefficients (Homand-Etienne & Houpert, 1989; Lin, 2002; Somerton, 1992). Thermal effects on granite primarily result in microcracks initiation, which governs many of its physical and mechanical properties. These microcracks-related effects in granite have been investigated in studies across various temperature ranges for example, 20–105°C (Freire-Lista et al., 2016), 20–500°C (Mo et al., 2022), 20–600°C (Alcock et al., 2023; Feng et al., 2023), and 20–800°C (Kumari et al., 2017; Yang et al., 2017). With increasing temperature, granite's physical properties, such as density, P-wave velocity, and thermal conductivity, decrease, while its volume and permeability behavior are significantly altered (Yang et al., 2020; Pan et al., 2023; Jin et al., 2019). Various methods are used to analyze microcracks, each offering unique advantages. These include SEM imaging (Durham et al., 1985), computed tomography (Fan et al., 2018), acoustic emission (Tronskar et al., 2003), X-ray diffraction (Zhang et al., 2019), thermomechanical analysis (Samouh et al., 2021), and micro-CT (Isaka et al., 2019). Microscopic examination, particularly with fluorescence microscopy, is a common approach for studying microcracks. Fluorescence microscopy employs tracers like fluorescein or rhodamine to highlight microcracks. Injecting these tracers into rock samples enhances visibility, allowing for detailed analysis. Petrographic and fluorescence microscopy, along with fracture analysis, are among the most effective methods for petrographic investigation (Freire-Lista et al., 2016). Important information regarding the effects of decay, particularly microcracking, can be obtained through fluorescence microscopy analysis (Murru et al., 2018). This method is instrumental in selecting granites suitable for construction in environments with high thermal stress (Sousa et al., 2005; Freire-Lista et al., 2016).

Nehbandan (NB), Natanz (NZ), Taibad (TB), and Khormadareh (KD) granites are among the most renowned Iranian granites, highly regarded in the stone industry for their aesthetic appeal, excellent technical properties, and widespread availability. These qualities make them some of the best-selling building materials in Iran. The granites of NB and NZ, with their white backgrounds; TB, featuring pink to peach tones; and KD, with a grayish background, are extensively used in the construction industry. Their durability, aesthetic qualities, and high resistance make them ideal for applications such as exterior and interior facades, flooring, and

stairs. Processed and distributed across numerous stone factories in Iranian cities, these granites are valued for their high quality.

This study investigates four widely used Iranian granites to assess the effects of thermal stress on their microcracks characteristics and physical properties across a range of temperatures. The research specifically aims to (1) analyze the evolution of thermal microcracks patterns, including type, density, and width, and (2) evaluate the resulting changes in porosity, water absorption, and P-wave velocity under dry and saturated conditions. To achieve these objectives, multiple laboratory tests were conducted. Thin sections were prepared and impregnated with a fluorescent tracer, allowing detailed observation and quantification of microcracks using petrographic and fluorescence microscopy. In addition, porosity, water absorption, and P-wave velocity tests were performed at controlled temperature intervals. By combining high-resolution imaging with quantitative physical measurements, this study presents a novel and comprehensive methodology for characterizing thermal damage in studied granites. Despite their commercial importance and widespread application, these four granite types have not previously been investigated using high-resolution techniques. This study is the first to characterize their thermal microcrack evolution in this level of detail, enabled by applying fluorescence tracer methods and integrated microscopy. Understanding these microcracks characteristics is crucial for evaluating granite performance in fire-prone environments and planning effective restoration strategies in historical or modern stone structures. While most previous studies have investigated thermal damage up to temperatures of around 800 °C, this research extends the analysis up to 1050 °C, providing new insights into the behavior of granites under extreme thermal conditions.

Materials and Methods

Sample Preparation

Granite samples, including those from NB, NZ, TB, and KD, were collected from stone processing factories located south of Tehran (Shurabad). The samples were prepared in the form of rectangular Cuboid with dimensions of 5×10×10 cm and tiles measuring 2×20×40 cm. These samples were sourced from active quarries in Iran, with their approximate locations indicated in Fig. 1. The extracted blocks varied in size. They were transported to stone-cutting factories for further processing. The tile samples were prepared with a single polished surface using standard polishing techniques. Before any treatments, the samples were cut into the specified dimensions at the Building Stones Laboratory of Tarbiat Modares University. The cutting dimensions for various tests are provided in Table 1.

Heating in the Furnace

The most crucial part of this study was applying heat to the granite samples. The samples were subjected to eight temperature stages: 20, 150, 300, 450, 600, 750, 900, and 1050 °C (Fig. 2).

Table 1. Number and dimensions of the cut samples for the various tests

Total cut specimens	Sample dimension (cm)	Test name
128 (32 cut specimens for each of 4 granite types)	2 (tile)×10×20	Heating in the Furnace
128 (32 cut specimens for each of 4 granite types)	2 (tile)×10×20	Water absorption, porosity, and density
96 (24 cut specimens for each of 4 granite types)	5 (Cuboid)×5×10	P-wave velocity
32 (8 cut specimens for each of 4 granite types)	2 (chips)×2×4	Fluorescence thin section

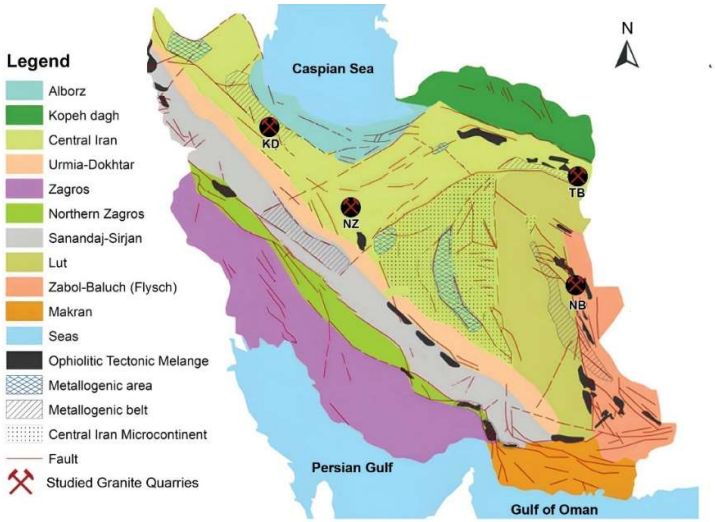

Figure 1. Geological locations of the quarries on Iran map corresponding to the granite samples, including KD in the east of Zanjan Province, NZ in the north of Isfahan Province, TB in the southeast of Razavi Khorasan Province, and NB in the south of South Khorasan Province, Iran

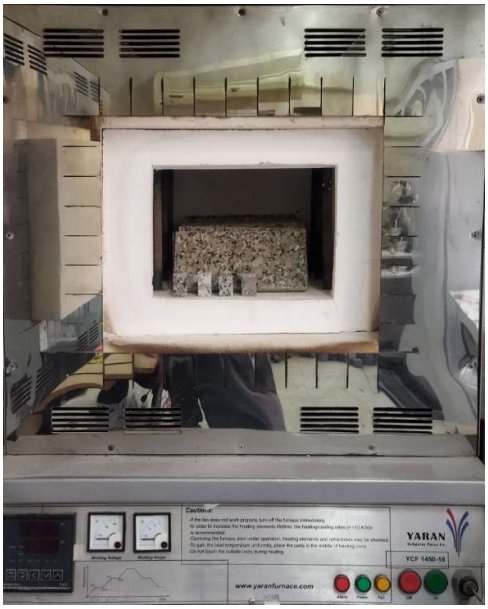

Figure 2. The furnace used in the experiment, equipped with a HANYOUNG controller, model PX

Following the methodology of Huang et al. (2017), these temperature intervals were deliberately selected to allow detailed observation of heat-induced changes at shorter and more precise thermal steps. The heating rate was set at 5 °C per minute to avoid the possible thermal shock that may occur under rapid heat development in the samples (Kumari et al., 2017). The samples were kept in the furnace for 4 hours to ensure uniform heat distribution (Huang et al., 2017). After this period, the furnace was cooled down at a rate of 5 °C per minute. It is important to note that the samples were exposed to ambient air after being removed from the furnace without experiencing thermal shock from being transferred to a different chamber or water tank. At each temperature stage, 4 tiles, 3 Cuboids, and 1 chip were selected from each type of granite and placed in the furnace. In total, 16 tiles, 12 Cuboids, and 4 chip samples from the four granite types were heated at each temperature stage.

Petrography properties: thin sections preparation using the fluorescence-dye epoxy injection method:

To prepare 32 microscopic thin sections with dimensions of 30 × 20 mm and a thickness of 30 µm (William *et al*., 1954) and study them under a fluorescence microscope, rectangular specimens (~3 × 2 × 1 cm) were precisely cut from the granite samples, ensuring that no secondary fractures were introduced during cutting. The least-deformed face of each specimen was gently ground using silicon carbide powder (mesh 800–1200), then rinsed under high-pressure water to eliminate fine abrasive particles from the pores. The specimens were subsequently dried in an oven at 105 °C for at least one hour. Following the methodology of zalooli et al. (2020), a fluorescence tracer (fluorescein) with a 5–10% concentration was mixed with diluted transparent epoxy resin. The mixture was optimized for both penetration and optical clarity. A small amount of this solution was applied to the specimen surface, and the samples were placed in a vacuum chamber at −0.8 bar for 10–15 minutes. Under this vacuum, the tracer–epoxy mixture deeply penetrated finer microcracks and pores. Then, the samples were cured in an oven at 50 °C for 24 hours. The excess cured resin was trimmed, and the impregnated surface was gradually polished using silicon carbide powders from mesh 100 to 1200 until a uniform, clean rock surface was exposed. A glass slide was then mounted onto the prepared face, and the unmounted side was thinned down by further grinding until a standard thickness of ~30 µm was achieved.

After these stages, the thin sections were prepared, and the samples were examined for petrographic analysis and microcracks evaluation using fluorescence and petrographic microscopes. The procedural steps are as follows:

On average, 100 images were captured at 10X magnification using a petrographic microscope (PM), with approximately 40% vertical and horizontal overlap of the thin sections. Additionally, 100 more images were captured at 10X magnification using a fluorescence microscope (FM), with approximately 20% vertical and horizontal overlap (zalooli et al., 2020). The scale of all captured images was 2 mm. An Olympus Bx 51 polarized light microscope, equipped with an Olympus ultraviolet lamp and an Olympus DP (6 V/2.5 Å) digital camera running version 3.2 of the DP-Soft Olympus software, was used to capture the images. The images were combined using Image Composite Editor software to produce separate PM and FM micrographs.

The FM micrographs were overlaid onto the corresponding PM micrographs using Photoshop software, enabling the simultaneous identification and examination of the microcracks in the FM images and the crystal texture in the PM images. At this stage, a red grid with five horizontal and vertical axes was applied to the final image.

Microcracks, represented in green, were quantified and classified by counting the number of microcracks that intersected with the sides of the red grid using JMicroVision software. As shown in Fig. 3, the microcracks were classified into three main categories as follows (Kranz, 1979; Freire-Lista et al., 2016):

Intra-crystalline: Microcracks found within individual crystals.

Inter-crystalline: Microcracks observed between adjacent crystals.

Trans-crystalline: Microcracks that pass through multiple crystals.

The number of each type of microcracks was determined relative to the total number of microcracks and expressed as the Intra-crystalline ratio, Inter-crystalline ratio, and Trans-crystalline ratio, in that order.

Similar to the studies of Ghasemi et al. (2020) and Sousa et al. (2005), the linear microcrack density (LMD), defined as the number of microcracks per unit length (mm), was determined and calculated to quantify and analyze the results.

The width of the studied microcracks was measured using JMicroVision software based on

Feret diameter method (Ruzyla, 1986; Ersoy & Waller, 1995; Berrezueta & Kovacs, 2017). Approximately 70 microcracks were measured in each micrograph. For each microcracks, a perpendicular line was manually drawn across the microcrack trace to represent its width, and the length of this line was recorded (Fig. 4). The average of these perpendicular line lengths was then calculated and reported as the microcracks width for each sample.

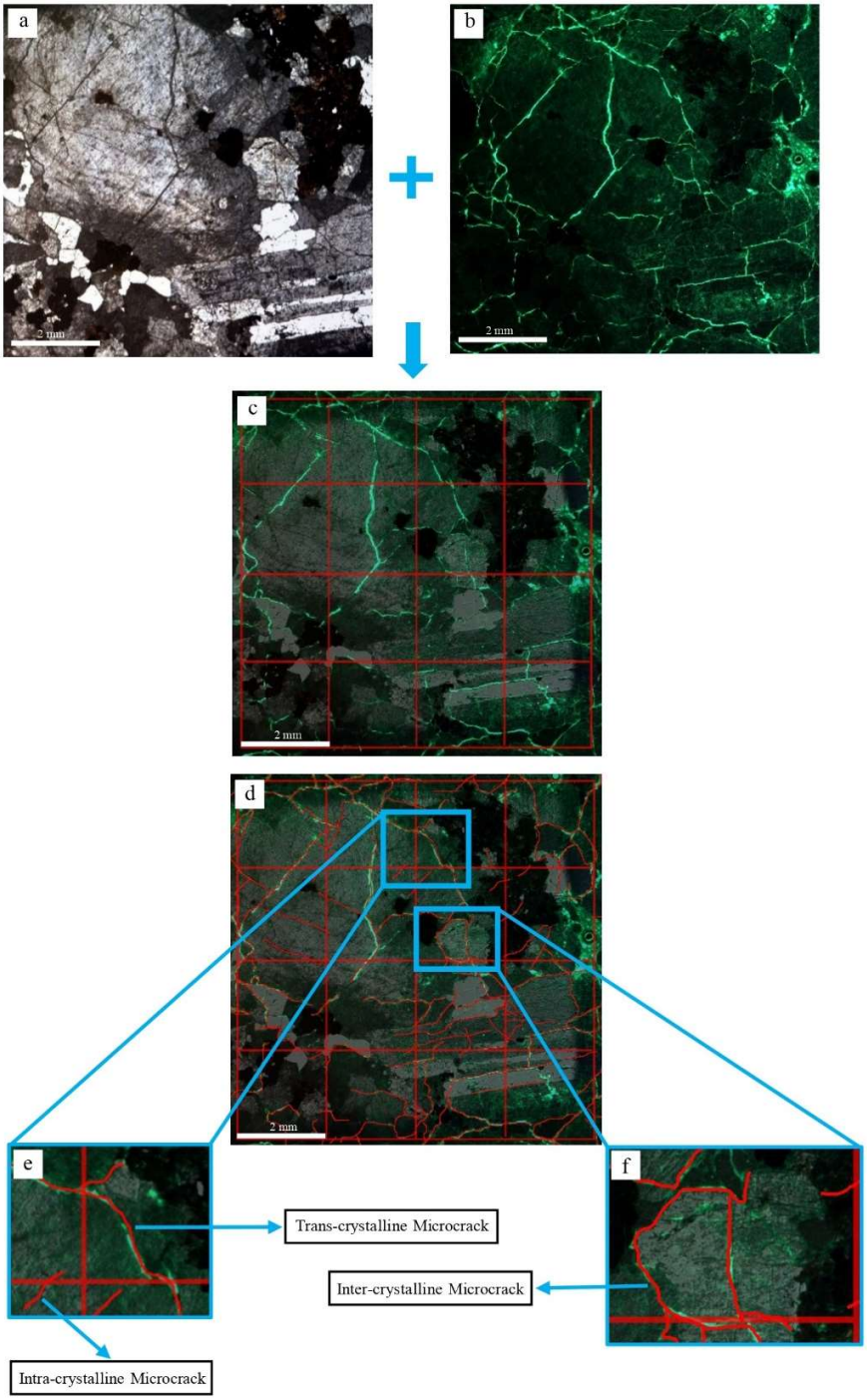

Figure 3. Thin section of KD sample after heating to 900 ˚C. FM microphotograph (b) overlaid on PM microphotograph (a) with an 8 × 8 mm grid subdivided into 2 × 2 mm squares (c), where red lines depict the microcracks types, including Intra-crystalline, Inter-crystalline, and Trans-crystalline (d, e and f)

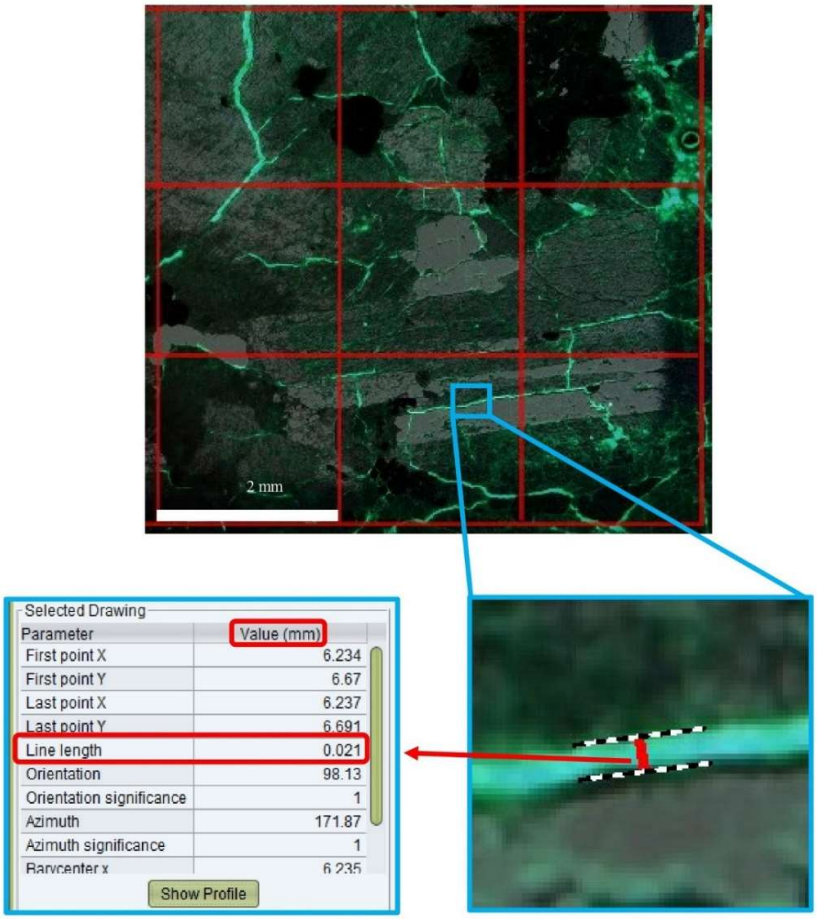

Figure 4. Example of microcrack width measurement using the Feret method in JMicroVision. Widths were measured by drawing perpendicular lines across microcracks

Physical properties

In total, 128 samples (32 cut samples from each of the four studied granites) with dimensions of 2 × 10 × 20 cm were used to determine physical properties after each temperature treatment. The physical properties measured included dry unit weight, water absorption by weight, and effective porosity of the samples, which were obtained using the saturation buoyancy test as per ISRM (2007). P-wave velocity measurements were performed according to ISRM (2007) using a Pundit Lab ultrasonic tester. The lateral minimum dimension (perpendicular to the direction of wave propagation) must be at least 10 times the wavelength (ISRM, 2007). Ultrasonic transducers with 36.77 mm and 44 mm diameters and 54 and 500 kHz frequencies were used to measure P-wave velocities in dry and saturated conditions, respectively. All samples had dimensions of 5 × 5 × 10 cm, which conform to ISRM standards. A gel-based couplant was applied between the transducer face and the stone surface to eliminate the air gap between the transducers and the specimen surface. These experiments were conducted after the samples were removed from the furnace and fully cooled.

Results

Petrological studies

The petrographic characteristics of the studied granite samples are presented in Table 2.

According to scientific classification, all four types of samples are categorized as granite (Fig. 5). The approximate percentage of constituent minerals in each granite was determined using the point-counting method (Philpotts & Ague, 2009). In the NB and NZ samples, quartz constituted the most significant volume of the rock; however, the quartz crystals in NB sample were, on average, approximately 1 mm larger than those in NZ sample, resulting in a visibly coarser-grained texture in hand specimens compared to NZ. In the KD and TB samples, feldspar group minerals were dominant. Notably, in the KD sample, orthoclase was the prevailing type of feldspar, whereas in the TB sample, microcline was dominant. The presence of orthoclase in KD imparts a predominantly grayish tone to the rock, whereas microcline in TB is responsible for its distinctive pink to peach coloration. Alterations observed in the KD, NZ, and TB samples were of the chloritization type, while carbonation and silicification were the dominant alteration types in the NB sample.

Thermal microcracks characteristics

The parameters for the microscopic analysis of thermal microcracks are provided in Table 3. This table presents the ratios of intra-crystalline, inter-crystalline, and trans-crystalline microcracks, along with the linear microcrack density (LMD), across temperatures ranging from 20°C to 1050°C.

Table 2. Petrographic characteristics of the KD, NB, NZ, and TB granites

Name	Texture	Crystal Size	Main Minerals	Main Minerals Percentage	Alteration
KD	Granular	Plagioclase (1 Mm -6.5 Mm) Alkaline Feldspar (1 Mm -8 Mm) Quartz (100 µm – 1.5 Mm) Biotite (100 µm – 2 Mm)	Plagioclase (Albite), Alkaline Feldspar (Orthoclase), Quartz, Biotite, and Opaque Minerals.	Quartz: 20 % Feldspar: 60 % Biotite: 10 %	Chloritization (with an abundance of about 5%) accompanied by minor amounts of clay minerals and calcite.
NB	Granular	Plagioclase (800 µm-6 Mm) Alkaline Feldspar (700 µm -7 Mm) Quartz (100 µm – 3 Mm) Biotite (400 µm – 2.5 Mm)	Plagioclase (Albite), Alkaline Feldspar (Microcline), Quartz, Biotite, and Opaque Minerals.	Quartz: 40 % Feldspar: 40 % Biotite: 10 %	Carbonation (with an abundance of approximately 5%) and silicification (with an abundance of approximately 5%) accompanied by minor amounts of chloritization and sericitization.
NZ	Granular	Plagioclase (700 µm-5.5 Mm) Alkaline Feldspar (1-7 Mm) Quartz (200 µm – 2 Mm) Biotite (300 µm – 2 Mm)	Plagioclase (Albite), Alkaline Feldspar (Orthoclase), Quartz, Biotite, and Opaque Minerals.	Quartz: 50 % Feldspar: 30 % Biotite: 10 %	Chloritization (with an abundance of approximately 5%) accompanied by minor amounts of calcitization, clay minerals, and epidotization.
TB	Granular	Plagioclase (800 µm-6 Mm) Alkaline Feldspar (1-11 Mm) Quartz (300 µm – 2.5 Mm) Biotite (300 µm – 1.5 Mm)	Plagioclase (Albite), Alkaline Feldspar (Microcline), Quartz, Biotite, and Opaque Minerals.	Quartz: 20 % Feldspar: 60 % Biotite: 10 %	Chloritization (with an abundance of less than 5%) accompanied by minor amounts of calcitization.

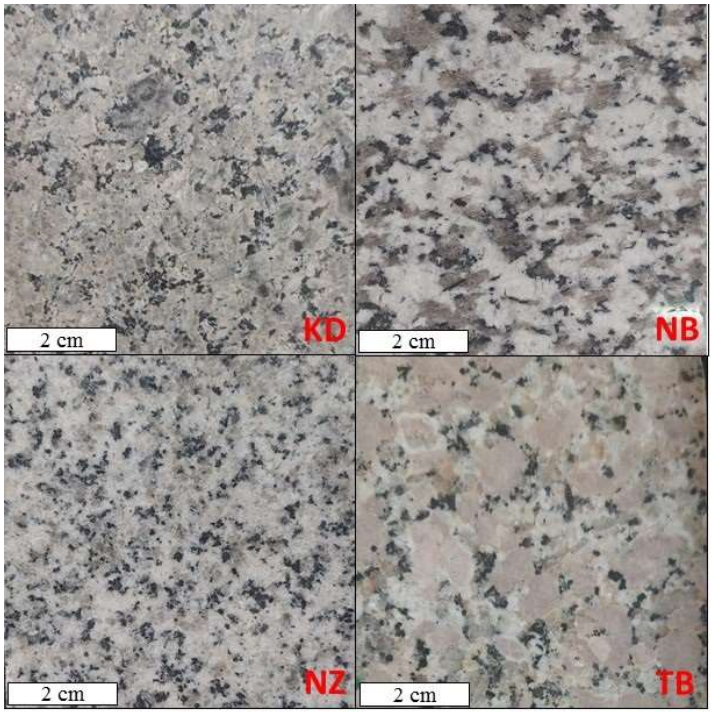

Figure 5. The textures and natural colors of the four granite types examined in this study before thermal treatment: (KD) with a grayish background, (NB) with a white background and relatively coarse-grained texture, (NZ) with a relatively fine-grained white background, and (TB) with pink to peach tones

Table 3. The ratio of thermal microcracks (intra-crystalline, inter-crystalline, and trans-crystalline) and the linear microcrack density (LMD) in KD, NB, NZ, and TB granite after exposure to temperatures ranging from 20°C to 1050°C

			TB					**KD**	
T (°C)	Intra-granular ratio	Inter-granular ratio	Trans-granular ratio	LMD	T (°C)	Intra-granular ratio	Inter-granular ratio	Trans-granular ratio	LMD
20	0.74	0.16	0.1	0.48	**20**	0.85	0.15	0	0.34
150	0.71	0.06	0.22	0.51	**150**	0.57	0.28	0.14	0.31
300	0.62	0.21	0.16	1.14	**300**	0.56	0.38	0.05	1.17
450	0.74	0.21	0.04	1.4	**450**	0.78	0.16	0.05	0.98
600	0.82	0.17	0	0.86	**600**	0.91	0.03	0.05	0.9
750	0.67	0.04	0.27	1.72	**750**	0.53	0.04	0.42	0.87
900	0.39	0.05	0.55	1.96	**900**	0.75	0.14	0.01	1.47
1050	0.59	0.03	0.37	2.71	**1050**	0.63	0.12	0.25	1.51
			NZ					**NB**	
T (°C)	Intra-granular ratio	Inter-granular ratio	Trans-granular ratio	LMD	T (°C)	Intra-granular ratio	Inter-granular ratio	Trans-granular ratio	LMD
20	0.77	0.22	0	0.46	**20**	0.61	0.27	0.16	0.36
150	1	0	0	0.32	**150**	0.8	0	0.2	0.76
300	0.7	0.1	0.2	1.33	**300**	0.8	0.12	0.07	1.48
450	0.86	0.11	0.03	1.11	**450**	0.39	0.12	0.49	0.73
600	0.77	0.19	0.02	2.56	**600**	0.72	0.11	0.16	1.51
750	0.66	0.18	0.14	3.25	**750**	0.61	0.01	0.36	0.83
900	0.63	0.1	0.26	2.48	**900**	-	-	-	
1050	0.62	0.09	0.28	1.56	**1050**	-	-	-	-

At room temperature, intra-crystalline microcracks represented the highest proportion, while trans-crystalline microcracks accounted for the lowest in all four granite types studied. The highest LMD was observed in TB granite, while the lowest was in KD granite. At 1050°C, the final thermal stage, intra-crystalline microcracks in TB, KD, and NZ granites maintained the highest proportion, similar to room temperature, while the ratio of trans-crystalline microcracks exhibited a considerable increase compared to room temperature. Due to severe degradation, it was not possible to measure the required parameters in NB granite at 900°C and 1050°C. Moreover, the LMD in all samples progressively increased with rising temperature up to 1050 °C (Fig. 6-a), demonstrating, overall, strong to moderate linear correlations ($R^2 = 0.7$ for KD and NB, 0.84 for TB and 0.51 for NZ). A comparable increasing trend was observed in the microcrack width of all samples, with values peaking at 1050 °C (Fig. 6-b) and in general, strong linear correlations were observed ($R^2 = 0.78$ for KD and NZ, 0.7 for TB, and 0.81 for NB). At room temperature NB granite exhibited the smallest microcrack, while KD granite showed the largest.

Physical Experiments

The physical experiments aimed to determine the mean values of water absorption, porosity, unit weight, and P-wave velocity. At room temperature (20°C), NB granite exhibited the highest water absorption and porosity (0.19% and 0.62% respectively), while TB granite showed the lowest (0.03% and 0.13% respectively). Additionally, NZ granite had the highest unit weight (26.40 kN/m^3), and NB granite had the lowest (25.76 kN/m^3). TB granite also demonstrated the highest P-wave velocity in dry and saturated conditions (5.48 and 5.68 km/s respectively), while NZ granite showed the lowest (3.98 and 4.99 km/s respectively). Due to significant degradation, standard porosity and water absorption measurements could not be taken for NB granite at 750°C and the other samples at 1050°C. The trend of changes in physical properties over the temperature range of 20°C to 900°C is presented in Fig. 7. In general, porosity and water absorption in the TB, KD, and NZ samples showed a strong positive correlation with increasing temperature from 20°C to 900°C. Specifically, porosity exhibits high linear regression coefficients for TB ($R^2 = 0.75$), KD ($R^2 = 0.72$), and NZ ($R^2 = 0.73$); similarly, water absorption shows strong correlations for TB ($R^2 = 0.76$), NZ ($R^2 = 0.72$), and moderate for KD ($R^2 = 0.55$). In contrast, the NB sample demonstrates no clear linear trend for porosity ($R^2 = 0.0008$) and only a moderate correlation for water absorption ($R^2 = 0.47$) (Figs. 7-a and 7-b, respectively). Moreover, unit weight, PWVD and PWVS generally decreased with increasing temperature from 20°C to 900°C, though the strength of the linear correlation varies across the granite types. For unit weight, moderate to strong negative correlations were observed in TB ($R^2 = 0.75$), NZ ($R^2 = 0.66$), and KD ($R^2 = 0.65$), indicating a consistent decrease with rising temperature. In contrast, NB ($R^2 = 0.11$) exhibited a very weak linear relationship (Fig. 7-c). For PWVD, moderate negative correlations were observed in TB ($R^2 = 0.67$), NZ ($R^2 = 0.6$), and KD ($R^2 = 0.53$), while NB ($R^2 = 0.03$) shows virtually no linear trend. In contrast, PWVS values exhibited strong negative correlations in TB ($R^2 = 0.86$) and NZ ($R^2 = 0.86$), followed by KD ($R^2 = 0.78$). However, NB again showed a very weak correlation ($R^2 = 0.06$) (Figs. 7-d and 7-e, respectively). In general, the magnitude of these changes became more pronounced beyond 600°C across all the studied properties.

Discussion

The Effect of Heat on Microcracks Characteristics

According to Table 3 and Fig. 6, as the temperature increased to 150 °C, no significant change

was observed in the LMD for most samples except for NB granite. The LMD in the NB sample showed a noticeable increase, rising from 0.36 to 0.76. This increase could be attributed to the coarser crystal size of this granite (as shown in Table 2).

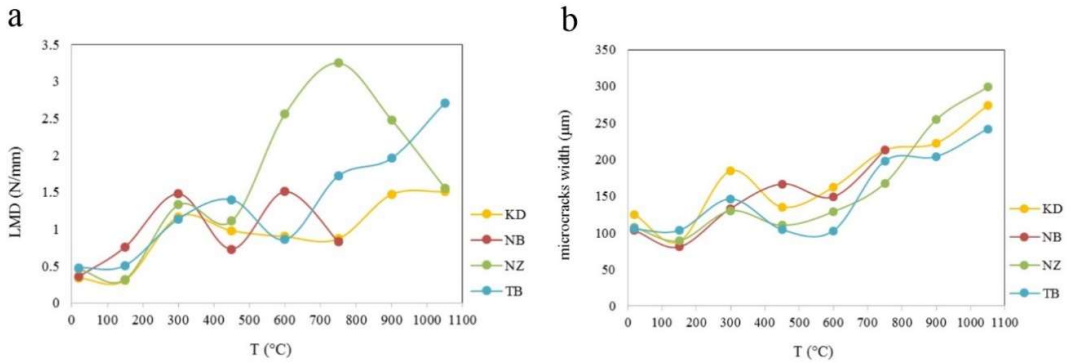

Figure 6. Variations of (a) LMD and (b) microcracks width (μm) with increasing temperature from 20 °C to 1050 °C in KD, NZ, TB, and NB granites. Both parameters increased as the temperature raised

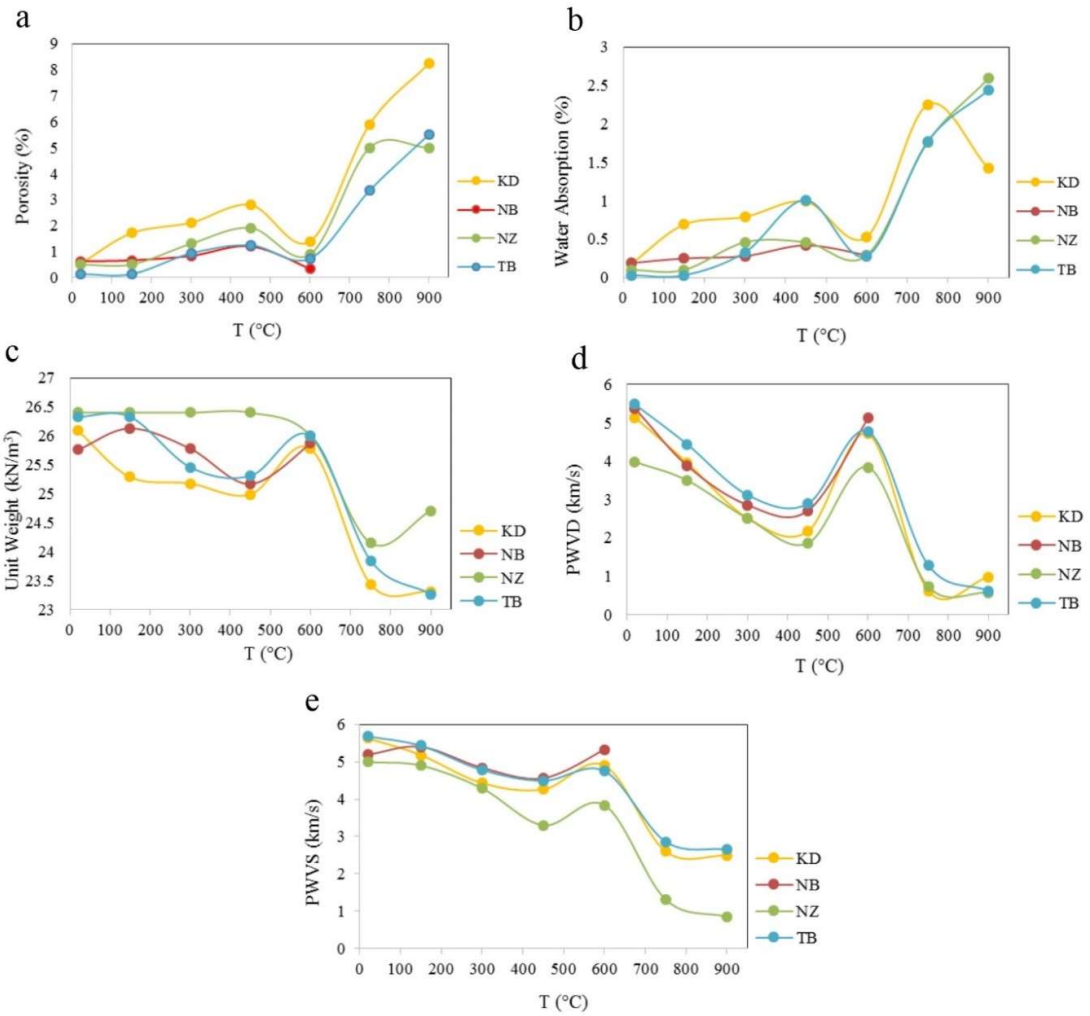

Figure 7. Relationship between increasing temperature (from 20 °C to 900 °C) and the evolution of physical properties, including (a) porosity, (b) water absorption, (c) unit weight, (d) P-wave velocity in dry condition (PWVD), and (e) P-wave velocity in saturated condition (PWVS), for KD, NB, NZ, and TB granite samples. Each data point represents the mean value of measurements

Shao et al. (2014) suggest that larger quartz crystals exhibit a more pronounced reaction to temperature changes. At this stage, the average width of microcracks in the KD, NZ, TB, and NB samples was 88.09, 89.22, 103.28, and 80.75 μm, respectively (the lowest values among all tested temperatures). The reduction in microcracks width at this temperature can be explained by the thermal expansion of mineral crystals, which tends to close microcracks.

A noticeable rise in LMD values was recorded from 150 °C to 300 °C in all granite types, increasing from 0.51 to 1.14 in TB, 0.31 to 1.17 in KD, 0.32 to 1.33 in NZ, and 0.76 to 1.48 in NB. This phenomenon, consistent with findings from Feng et al. (2023), can be attributed to a substantial rise (at least twofold) in the thermal expansion of quartz and feldspar minerals (Clark, 1966). At this temperature, the proportion of intra-crystalline microcracks decreased upon cooling in the TB, KD, and NZ granites (dropping from 0.71 to 0.62, 0.57 to 0.56, and 1.00 to 0.7, respectively) while remaining unchanged at 0.8 in the NB granite. Conversely, the proportion of inter-crystalline microcracks increased in the TB, KD, NZ, and NB granites (rising from 0.06, 0.28, 0.0, and 0.0 to 0.21, 0.38, 0.1, and 0.12, respectively).

At 450 °C, the LMD decreased in all granite samples except for TB, which increased to 1.4. In contrast, the values declined to 0.98 in KD, 1.11 in NZ, and 0.73 in NB, likely due to the closure of microcracks caused by thermal expansion. However, the NB sample exhibited a more significant decrease in LMD, which could be attributed to its relatively larger crystal sizes (100 μm – 3 mm). In the NB sample, the ratio of trans-crystalline microcracks increased (from 0.07 to 0.49), indicating weakening in its microstructure (Yang et al., 2020), while in the TB, KD, and NZ samples, the ratio of intra-crystalline microcracks increased (0.74, 0.78 and 0.86, respectively).

At 600 °C, the LMD increased significantly in the NB and NZ samples, rising from 0.73 to 1.51 and 1.11 to 2.56, respectively. This substantial rise is attributed to the higher quartz content in these granites, approximately 40% in NB and 50% in NZ (Table 2). Quartz undergoes a phase transition from alpha to beta at 573 °C, causing significant volume changes in its crystal structure (Alcock et al., 2023; Feng et al., 2023; Gómez-Heras et al., 2010; Štubňa et al., 2007; Yang et al., 2020). This transition led to high-stress concentrations within the quartz crystals, forming a network of inter-crystalline microcracks around them and numerous intra-crystalline microcracks within them (Fig. 10-b). In contrast, the TB and KD samples exhibited a slight decrease in LMD (from 1.4 to 0.86 and 0.98 to 0.9, respectively).

At 750 °C, the NB Cuboid and tile specimens collapsed (Fig. 8). In the NB sample, despite a decrease in LMD (from 1.51 to 0.83), the ratio of trans-crystalline microcracks slightly increased (from 0.16 to 0.36), contributing to the specimen's collapse. The larger quartz crystals in the NB sample (100 μm – 3 mm) made it more susceptible to heat. Inter-crystalline and intra-crystalline microcracks at this temperature were interconnected, extending the trans-crystalline microcracks (Fig. 10-a). In the NZ sample, the LMD increased significantly (from 2.56 to 3.25), with no notable changes in the ratio of different microcracks types. The KD granite sample showed a relatively constant LMD. At the same time, the ratio of trans-crystalline microcracks increased (from 0.05 to 0.42), likely due to the connection of intra-crystalline and inter-crystalline microcracks. The TB sample exhibited an increase in LMD (from 1.72 to 2.07). Across all samples, the ratio of intra-crystalline microcracks decreased as trans-crystalline microcracks became more prevalent (Table 3). At this temperature, the average width of microcracks increased significantly in all samples (Fig. 9). In the TB, KD, NZ, and NB granites, the average width rose from 102.88 to 197.99 μm, 162.18 to 212.74 μm, 128.85 to 167.61 μm, and 149 to 212.88 μm, respectively.

At 900 °C, the LMD increased in the TB and KD samples (from 2.07 to 2.96 and 0.87 to 1.47, respectively) while it decreased in the NZ sample (from 3.25 to 2.48). The width of microcracks increased in all three samples (Fig. 6-b), and many trans-crystalline microcracks were interconnected, further contributing to microstructural changes.

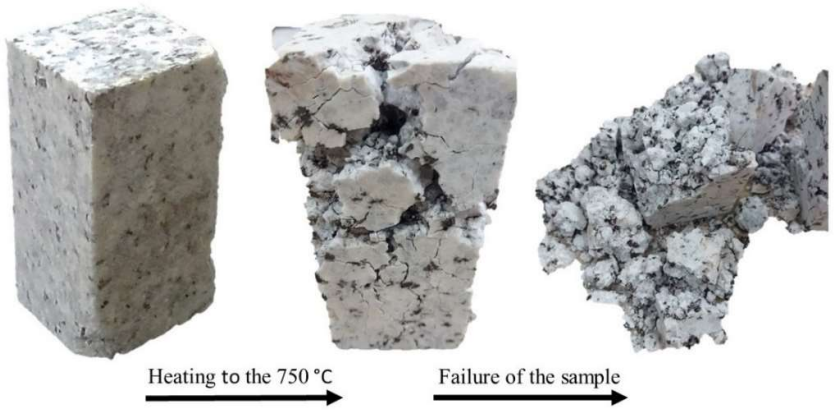

Figure 8. Failure of the NB granite specimens at 750 °C due to intense thermal stress and internal microcracking

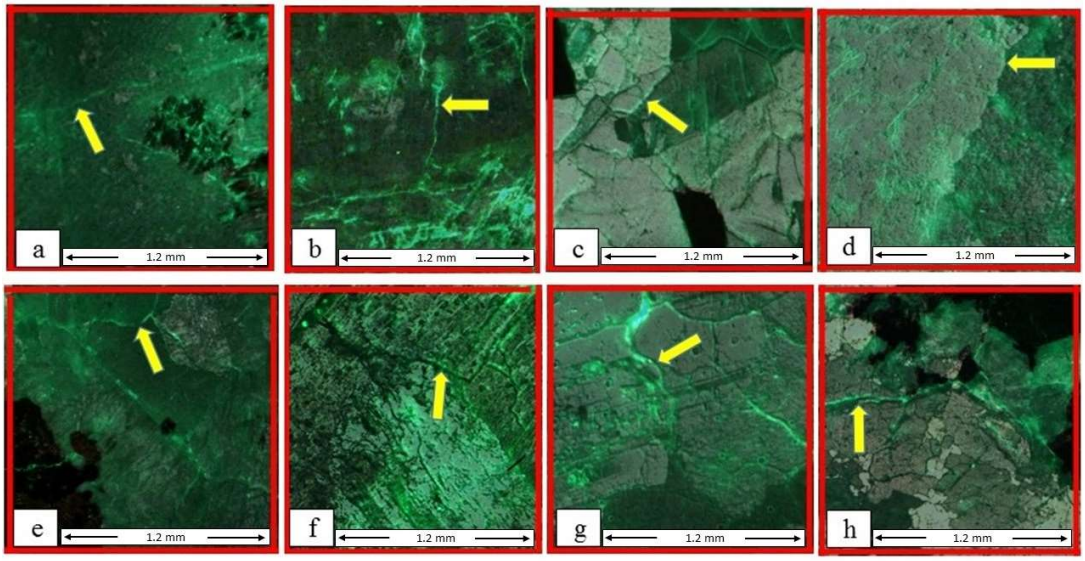

Figure 9. Micrographs showing the microcracks widths in the granite samples at 600 °C (a–d) and 750 °C (e–h). KD: (a, e), NB: (b, f), NZ: (c, g), and TB: (d, h). Yellow arrows indicate the microcracks, which increased in width at 750 °C compared to 600 °C

At 1050 °C, the final temperature step, the LMD increased in the TB sample (from 2.96 to 3.71) but showed a slight decrease in the NZ sample (from 2.48 to 1.56). A marginal increase in LMD was also observed in the KD sample (from 1.47 to 1.51). Like the conditions at 900 °C, extensive interconnections between trans-crystalline microcracks were evident at this temperature.

Thermal changes, particularly at high temperatures, significantly affect the microcracks and granite's physical and mechanical properties. This phenomenon is primarily attributed to variations in the thermal expansion coefficients of the minerals comprising granite. As Skinner (1966) explains, minerals' differing thermal expansion rates lead to uneven expansion and deformation. Upon cooling to room temperature, the deformation caused by thermal expansion becomes irreversible (Feng et al., 2023). Analysis of the four studied granites shows that the number and width of microcracks increase with rising temperatures. According to Yin et al. (2016), thermal damage in granite is more pronounced at lower temperatures than higher ones. Quartz crystals play a key role in this microcracking process (Huang & Li, 2023) because they exhibit the highest coefficient of thermal expansion among the constituent minerals of granite (Skinner, 1966; Vázquez et al., 2015).

Examining the types and ratios of microcracks across different temperatures in this study highlights the significant influence of quartz and feldspar minerals. Quartz, with its high thermal expansion coefficient, anisotropic thermal behavior, and multiple crystal phases, undergoes intense stress concentrations (Van der Molen, 1981). These stresses manifest as intra-crystalline microcracks within quartz grains (Fig. 10-b). At elevated temperatures, these microcracks propagate into adjacent grains, forming trans-crystalline microcracks (Fig. 10-a). In samples with lower quartz content, feldspar minerals play a dominant role in forming intra-crystalline microcracks (Fig. 10-c). Although feldspar's thermal expansion coefficient is lower than that of quartz, its weak surfaces, such as twinning and cleavage planes, combined with crystallographic anisotropy and secondary mineral phases, facilitate the development of fine microcracks, particularly inter-crystalline ones (Freire-Lista et al., 2016; Vázquez et al., 2015). Mica group minerals, such as biotite, act as stress concentrators due to the thermal expansion of surrounding minerals. While these stresses do not produce a distinct microcracks system within the mica itself (Fig. 10-d), they lead to extensive microcracking in adjacent crystals, serving as propagation centers for microcracks (Vázquez et al., 2015).

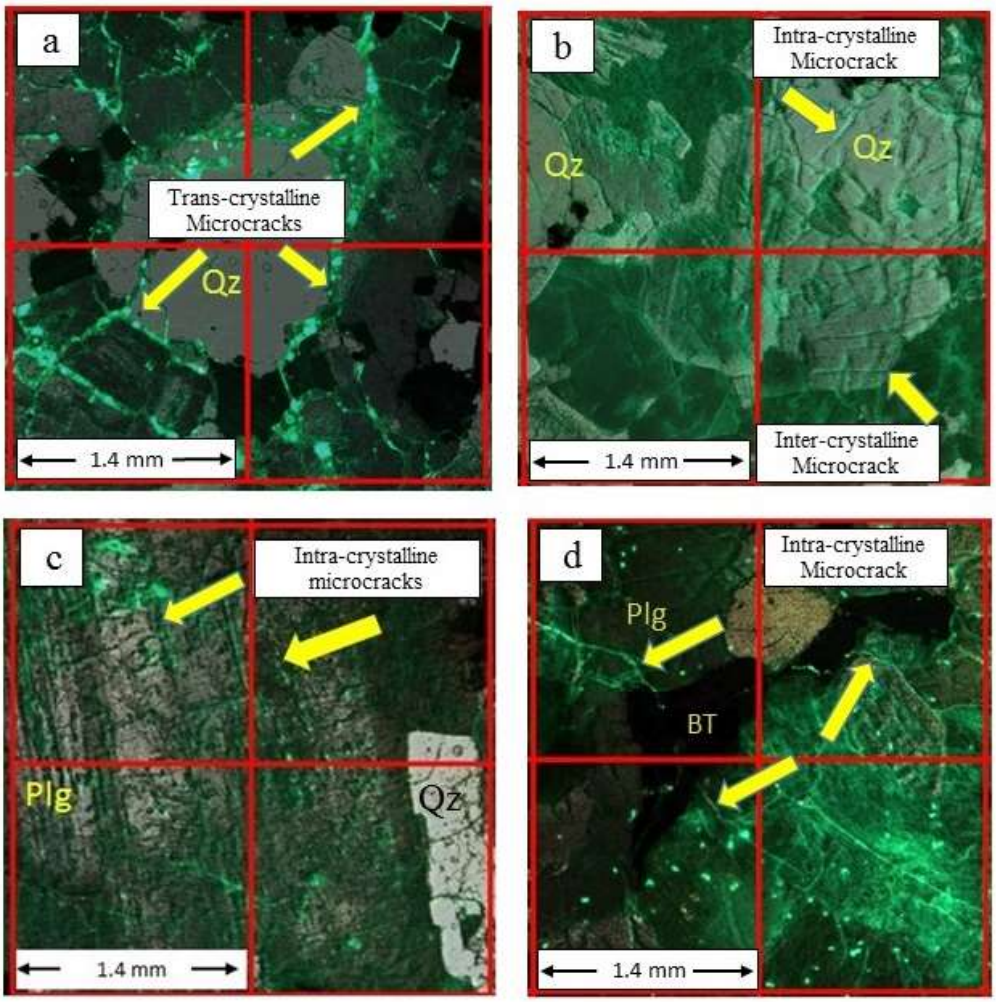

Figure 10. a) Connection of trans-crystalline microcracks surrounding the quartz mineral at 750°C in the NB sample. b) Formation of extensive intra-crystalline and inter-crystalline microcracks within the quartz mineral at 600°C in the NZ sample. c) Development of multiple intra-crystalline microcracks within the plagioclase mineral at 300°C in the KD sample. d) Microcracks around the biotite mineral are concentrated, highlighting their resistance to microcracks development at 300°C in the NB sample. Yellow arrows indicate the different types of microcracks

Thermal Effects on Physical Properties Including Porosity and Water Absorption

Microcracking, the primary impact of heat on granite, significantly influences its physical properties, including porosity, water absorption, and unit weight. As shown in Figs. 11-a and 6-a, in the KD sample, with increasing temperature up to 300 °C, the LMD exhibited a noticeable increase from 0.34 to 1.17. In contrast, the changes in porosity and water absorption were relatively moderate, increasing from 0.52% at 20 °C to 1.71% at 150 °C and 2.11% at 300 °C for porosity, and from 0.18% at 20 °C to 0.69% at 150 °C and 0.79% at 300 °C for water absorption. Although the average width of microcracks increased from 88.09 µm at 150 °C to 184.55 µm at 300 °C, the limited increase in porosity and water absorption suggests that the microcracks remained poorly connected. This is likely due to the early stage of thermal expansion in minerals such as quartz and feldspar, which produced isolated rather than interconnected microcracks (Shi et al., 2020). At 450 °C, the LMD decreased slightly, but both porosity and water absorption increased. Porosity reached 2.79%, representing a 436.5% increase compared to its initial value at 20 °C (0.52%), while water absorption rose to 0.99%, marking a 450% increase from its original value of 0.18% at 20 °C. The sharp rise in porosity and water absorption, despite a slight decrease in LMD, may be attributed to the formation of wider or more open microcracks rather than an increased number of them (Gao et al., 2021). At 600 °C, the volume changes in quartz caused a decrease in porosity (1.39%) and absorption (0.53%). At 750 °C, a sudden increase in porosity and water absorption was observed (5.9% and 2.25%, respectively), while the number of microcracks did not change significantly compared to 600 °C. Finally, at 900 °C, the highest LMD and the greatest porosity were observed due to increased trans-crystalline microcracks with large widths. The porosity reached 8.25%, representing an increase of approximately 1486.5% compared to 20 °C (Fig. 7-a). The decrease in water absorption at this temperature (from 2.25% at 750 °C to 1.42% at 900 °C) may be attributed to the fact that microcracks, with large widths and well-established connections, do not retain much water and therefore have little impact on water absorption (Mao et al., 2023; Wang & Bao, 2019).

In the NB granite (Fig. 11-b), as the temperature increased from room temperature to 300 °C, LMD, porosity, and water absorption increased consistently. Porosity increased from 0.62% at 20 °C to 0.83% at 300 °C, representing an approximate 34% increase. Water absorption rose from 0.19% at 20 °C to 0.28% at 300 °C, showing about a 47% increase. Despite the slight decrease in LMD at 450 °C (Fig. 6-a), the continued increase in porosity (1.2%) and water absorption (0.42%) suggests that microcracks became wider or more open rather than more numerous, likely enhancing fluid penetration. At 600 °C, the phase change of quartz led to an increase in intra-crystalline microcracks in this mineral, resulting in an overall increase in LMD. However, these microcracks had little effect on porosity and water absorption, as these values decreased to 0.33% and 0.29%, respectively. In other words, the width and connectivity of the microcracks appear to play a more significant role in controlling water absorption, while the number of microcracks governs porosity.

In the NZ sample (Fig. 11-c), as the temperature increased to 750 °C, LMD showed a general upward trend. However, it slightly decreased at 150 and 450 °C (Fig. 6-a), likely due to differences in petrological characteristics within the same rock type. Both porosity and water absorption also increased up to 750 °C. Porosity rose from 0.5% at 20 °C to 5.0% at 750 °C (an increase of 900%), while water absorption increased from 0.1% to 1.76% (an increase of 1660%). However, at 600 °C, quartz phase changes led to decreased porosity and water absorption (0.89% and 0.29%, respectively). At 900 °C, while LMD decreased, porosity remained unchanged compared to the previous temperature (5 %), as the same few microcracks created larger pore spaces in the rock due to their wider width. Furthermore, water absorption continued to rise (from 1.76% to 2.59%), suggesting that the width of the microcracks is sufficient to hold water within their spaces.

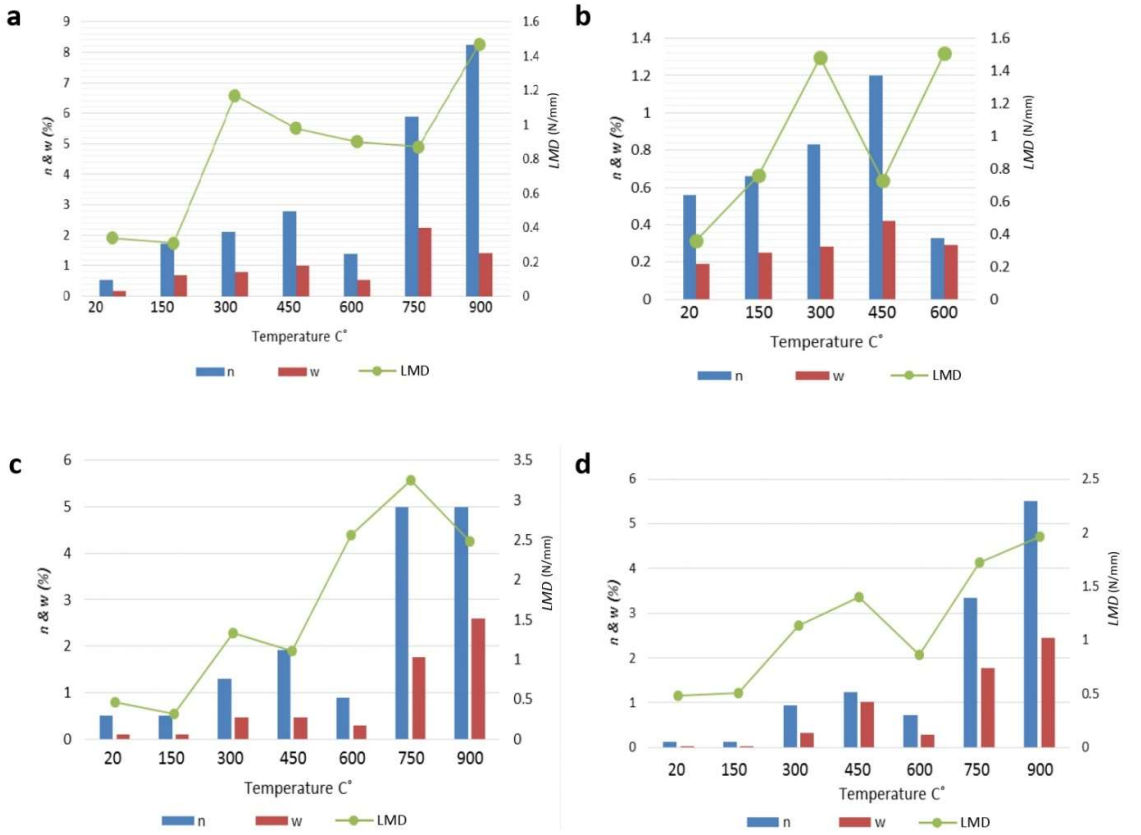

Figure 11. Changes in porosity (n: blue bar), water absorption (w: red bar), and LMD (green line) at temperatures ranging from 20°C to 900°C for a) KD, b) NB, c) NZ, and d) TB granites. The vertical axis on the left side represents changes in porosity and water absorption, while the vertical axis on the right represents changes in LMD. The horizontal axis indicates the temperature changes

As the temperature of the TB sample increased to 450 °C, all three parameters (LMD, porosity, and water absorption) also increased. Porosity rose from 0.13% at 20 °C to 1.24% at 450 °C (an increase of approximately 854%), while water absorption increased from 0.03% to 1.01% (an increase of approximately 3267%). However, at 600 °C, all three parameters exhibited a decrease; Porosity dropped to 0.73% (a decrease of approximately 41% compared to 450 °C), and water absorption decreased to 0.28% (a reduction of about 72%). As illustrated in Fig. 11-d, LMD significantly influenced porosity and water absorption in TB granite.

Analysis of the graphs in Fig. 11 reveals that the first significant increase in LMD across all four studied granites occurs at 300°C. At this temperature, the LMD in the KD, TB, NZ, and NB samples increased by 3.77, 2.23, 4.15, and 1.94 times, respectively, compared to the 150°C samples. These findings align with observations from other studies (Zhao et al., 2024; Gomah et al., 2024). At this temperature, the proportion of inter-crystalline microcracks increases in all samples, while the proportions of intra-crystalline and trans-crystalline microcracks either decrease or remain constant. Additionally, the average width of microcracks in the KD, TB, NZ, and NB samples increased from 88.09, 103.28, 89.22, and 80.75 µm to 184.09, 146.28, 130.05, and 133.24 µm, respectively. Consequently, porosity and water absorption also increased at 300°C. However, Gomah et al. (2024) identified 400°C as the critical temperature for a significant increase in porosity.

The temperature of 600°C represents a critical threshold for the LMD, porosity, and water absorption parameters in the four studied granite samples. At this temperature, a significant reduction in porosity and water absorption is observed, which can be attributed to the phase

transition of quartz at 573°C. This transition induces substantial volumetric changes in quartz, resulting in the dominance of intra-crystalline microcracks across all samples (Table 3). While the LMD remains relatively high at this stage, the intra-crystalline microcracks contribute minimally to porosity and water absorption compared to other microcracks types. As a result, the values for these two parameters reach their lowest levels at 600°C.

Conversely, at 750°C, there is a significant increase in both porosity and water absorption across all samples except for NB granite. This behavior correlates with a marked rise in the proportion of trans-crystalline microcracks. Between 600°C and 750°C, the proportion of trans-crystalline microcracks in KD, TB, NZ, and NB granites increases from 0.05, 0, 0.02, and 0.16 to 0.42, 0.27, 0.14, and 0.36, respectively. Trans-crystalline microcracks, predominantly formed at higher temperatures, have been identified as the key factor driving the increased porosity and water absorption (Zhao et al., 2024; Ahmadi et al., 2023). The behavior of the NB granite at 600°C is unique, as thermal stresses exceed the rock's strength, leading to structural disintegration and failure. This phenomenon is attributed to the expansion and dominance of trans-crystalline microcracks at this temperature (Feng et al., 2023).

At 750°C, the average width of microcracks in KD, TB, NZ, and NB granites reaches 212.74, 197.99, 167.61, and 212.88 μm, respectively. This increase in microcracks width, driven by elevated temperatures and thermal stress, significantly contributes to the rise in both porosity and water absorption values. Below 600°C, the increase in microcracks width has a negligible impact on porosity and water absorption. However, 750°C marks a critical threshold for average microcracks width, where its influence becomes more pronounced. This temperature correlates with a substantial increase in porosity and water absorption. It is important to note that other studies have identified lower temperature thresholds for microcracks width. For example, Feng et al. (2014) reported this threshold at approximately 300°C, while Homand & Houpert (1989) found it around 400°C.

Thermal Effects on P-wave velocity

The effect of temperature on rock fabric and the resulting deterioration before and after heat treatment can be assessed using P-wave velocity tests (Crosby et al., 2018; Wu et al., 2019; Yin et al., 2018). Overall, with increasing temperature, both P-wave velocity in dry (PWVD) and saturated (PWVS) conditions decrease (Jin et al., 2019; Pan et al., 2023). Additionally, porosity and water absorption influence P-wave velocity, as increased porosity typically reduces wave speeds due to greater microcracks connectivity and fluid presence (Ahmadi et al., 2023; Zhang et al., 2018)

In the case of KD granite (Fig. 12-a), as the temperature increased from 20°C to 450°C, both PWVD and PWVS exhibited a downward trend. Specifically, the PWVD decreased from 5.14 km/s to 2.17 km/s, and the PWVS dropped from 5.63 km/s to 4.26 km/s. This decrease correlates well with the concurrent increase in porosity and water absorption (Figs. 7-a and 7-b), facilitating wave attenuation by increasing fluid pathways and microcracks interconnectivity. However, at 600°C, a noticeable jump in both conditions was observed; the PWVD increased to 4.71 km/s, and the PWVS rose to 4.9 km/s. This increase corresponds with decreased porosity and water absorption, as quartz phase transition induces volumetric expansion and densification of the rock fabric, reducing fluid pathways and partially closing microcracks, thereby facilitating faster wave propagation. Subsequently, At 750°C, the significant decrease in PWVD and PWVS corresponds with a sharp increase in porosity due to extensive microcracks growth and coalescence, which reduces the rock’s density and wave propagation efficiency. At this stage, PWVD dropped to 0.62 km/s and PWVS to 2.60 km/s. At 900°C, although LMD slightly increased (Fig. 6-a), PWVS remained nearly constant compared to 750°C, while PWVD increased slightly.

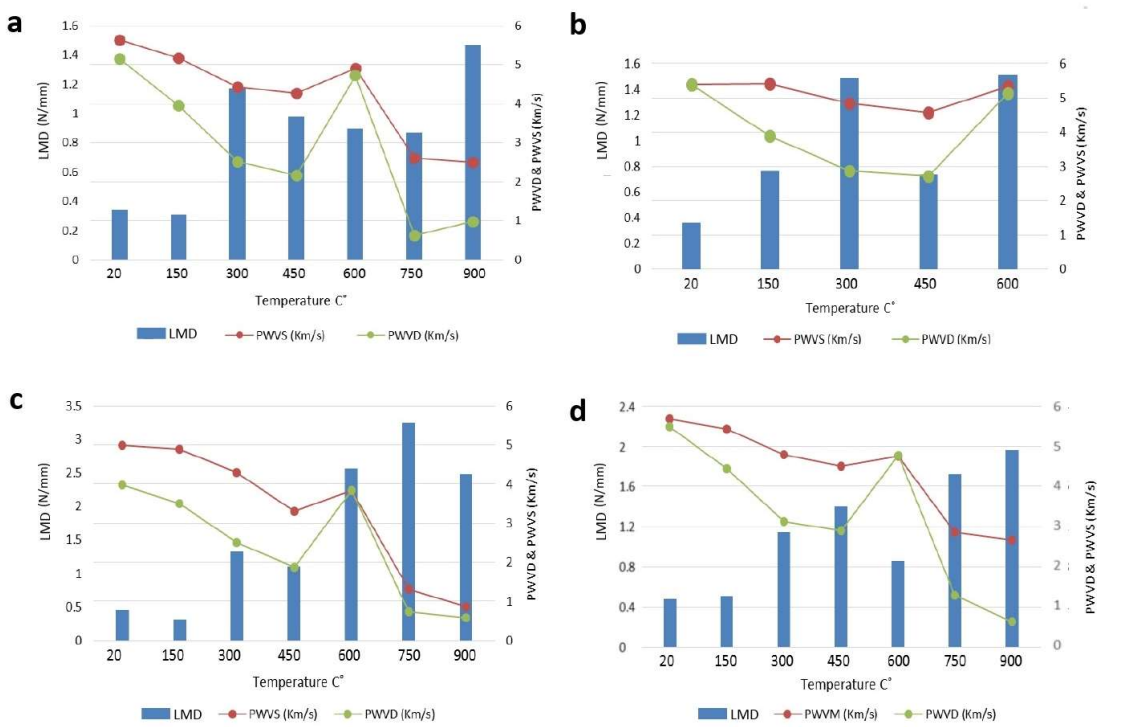

Figure 12. Changes in P-wave velocity under dry (PWVD: green line) and saturated (PWVS: red line) conditions, and LMD (LMD: blue bar) at temperatures ranging from 20 to 900 °C for a) KD, b) NB, c) NZ, and d) TB granites. The vertical axis on the left represents changes in LMD, while the vertical axis on the right represents changes in PWVD and PWVS. The horizontal axis indicates the temperature variations

The behavior of PWVD and PWVS in NB granite (Fig. 12-b) followed a similar trend to that of KD granite. However, the decrease in velocity from 20°C to 450°C was less pronounced (PWVD dropping from 5.38 to 2.71 km/s and PWVS from 5.19 to 4.56 km/s.), which can be attributed to the more minor changes in porosity in NB granite compared to KD granite (from 0.62% to 1.2% in NB versus 0.25% to 2.79% in KD). At 600°C, despite the increase in LMD, most microcracks were intra-crystalline, having minimal effect on P-wave velocity. As a result, both PWVD and PWVS exhibited an upward trend, reaching 5.12 km/s and 5.33 km/s, respectively.

For NZ granite (Fig. 12-c), PWVD and PWVS decreased with increasing temperature up to 450°C, dropping from 3.98 to 1.86 km/s and 4.99 to 3.3 km/s, respectively. At 600°C, the rock became denser, and the P-wave velocities in both dry and saturated conditions converged, with both PWVD and PWVS reaching 3.84 km/s. At 750°C and 900°C, significant reductions in both PWVD and PWVS were observed, with PWVD decreasing to 0.73 km/s and 0.57 km/s and PWVS dropping to 1.31 km/s and 0.85 km/s, respectively. Meanwhile, porosity remained around 5%, representing the highest value recorded for this sample.

The P-wave velocity behavior in TB granite closely mirrors that of KD granite (Fig. 12-d). Like KD, PWVD and PWVS decreased to 450°C, reaching 2.89 km/s and 4.49 km/s, respectively. At 600°C, both velocities increased, with PWVD reaching 4.77 km/s and PWVS 4.75 km/s. However, a sharp decline was observed at 750°C and 900°C. At 750°C, PWVD and PWVS dropped to 1.29 km/s and 2.86 km/s, and further decreased at 900°C to 0.62 km/s and 2.65 km/s, respectively. A more pronounced difference between dry and saturated velocities was noted at 900°C, reflecting the rock's progressive structural degradation.

At 600°C, a relative increase in P-wave velocity was observed across all the studied samples.

This temperature, close to the phase transition of quartz (573°C), induces volumetric expansion in the rock's crystalline structure, increasing density. Consequently, porosity at this temperature is significantly reduced compared to 450°C (Fig. 7-a). Several studies confirm that decreased porosity increases PWVD and PWVS (Ahmadi et al., 2023; Zhang et al., 2018). Additionally, the highest proportion of intra-crystalline microcracks at this temperature minimally impacts P-wave velocity.

By analyzing the PWVD and PWVS graphs of the four granites (Fig. 12), it can be concluded that the P-wave behavior in all four samples is quite similar, up to 600°C. This similarity is also reflected in their porosity and water absorption trends, which remain relatively stable up to 600°C (Fig. 7-a). Beyond this temperature, significant microcracks growth increases porosity and fluid connectivity, resulting in corresponding changes in P-wave velocities. The key variation occurs at temperatures of 750°C and 900°C. According to Alcock et al. (2023), the most significant decrease in P-wave velocity occurs between 700°C and 800°C, which can be attributed to the expansion of microcracks from the phase transition of quartz, microcracks growth in plagioclase and mica deformation at high temperatures. The results suggest that the significant reduction in wave velocity at 750°C and 900°C is primarily due to trans-crystalline microcracks (Jiang et al., 2023; Shen et al., 2020; Shen et al., 2021; Vázquez et al., 2010), whose proportions notably increase at these temperatures (Table 3). Furthermore, the substantial increase in microcracks widths at these temperatures - reaching 212.74 μm for KD, 167.61 μm for NZ, 197.99 μm for TB, and 212.88 μm for NB at 750°C, and 222.28 μm for KD, 254.38 μm for NZ, and 204.01 μm for TB at 900°C - plays a crucial role in the reduction of both PWVD and PWVS (Ahmadi et al., 2023; Vázquez et al., 2010). The PWVD and PWVS behavior at 600°C further supports this finding, as most of the microcracks at this temperature are intra-crystalline.

In the case of NB granite, PWVD and PWVS could not be measured at temperatures above 600°C due to significant temperature-induced damage. For NZ granite, the decrease in PWVS above 600°C was more pronounced, resulting in a minor difference between PWVD and PWVS. It should be noted that NZ granite exhibited the highest LMD at 600°C, 750°C, and 900°C among all the samples studied (Fig. 6-a), indicating significant internal structural degradation of the sample. This explains the lower wave velocity at these temperatures compared to the other samples.

It should be noted that the present study had certain limitations. One of the most significant constraints was the severe microcracking and disintegration of the NB samples at 750 °C, which rendered the measurement of their physical properties at 750 °C and 900 °C unfeasible. Moreover, although microcracks analysis was conducted at 1050 °C in NZ, TB, and KD samples, standard physical property measurements could not be performed at this temperature due to extensive sample damage. As a result, the analysis of the relationship between microcracks development and physical properties was limited to the temperature range of 20 °C to 900 °C in mentioned samples.

Another limitation concerns the two-dimensional framework used for microcracks analysis. Microcracks develop and propagate in three-dimensional space and can influence the physical behavior of the rock in complex ways. However, due to constraints in thin section preparation and the capabilities of available microscopy techniques, only the characteristics and frequency of microcracks in two dimensions were examined in the present study.

Conclusions

In this study, microcracks formed in KD, NB, NZ, and TB granites at temperatures ranging from 20°C to 1050°C were analyzed using fluorescence microscopy. The effects of these microcracks on porosity, water absorption, and P-wave velocity were thoroughly investigated,

yielding significant insights. The findings reveal that the number and width of microcracks increase with rising temperatures, significantly influencing key properties such as linear microcrack density (LMD), porosity, water absorption, and P-wave velocity. Specifically, LMD increased by nearly 5.6 times in TB, 4.4 times in KD, and 3.4 times in NZ by 1050°C, while in NB granite, it rose to approximately 2.3 times its original value by 750°C. Porosity increased substantially by over 8 times in TB, 5.5 times in KD, and 10 times in NZ between 20°C and 900°C. In NB granite, porosity almost doubled by 600°C. Likewise, water absorption increased by nearly 8 times in KD, 13.5 times in TB, and 26 times in NZ, while in NB, it rose to about 1.5 times its original value by 600°C. These proportional increases underscore the significant impact of thermal microcracking on the structural and physical integrity of granitic rocks at elevated temperatures.

Quartz, the primary mineral with the highest thermal expansion coefficient, is critical in initiating and propagating microcracks, particularly during the alpha-to-beta phase transition at 573°C. This phase transition induces considerable stress concentrations in quartz crystals, leading to the formation of intra-crystalline microcracks. At higher temperatures, these microcracks expand into inter-crystalline and trans-crystalline systems.

At 300°C, all granite samples exhibit a notable increase in LMD and microcracks width, accompanied by a shift from intra-crystalline to inter-crystalline microcracks. Specifically, LMD increased from 0.34 to 1.17 in KD, 0.36 to 1.48 in NB, 0.46 to 1.33 in NZ, and 0.48 to 1.14 in TB. Similarly, the average microcracks width increased from 125.07 to 184.55 μm in KD, from 103.18 to 133.24 μm in NB, from 107.58 to 130.05 μm in NZ, and from 105.10 to 145.28 μm in TB. This change is attributed to the thermal expansion of quartz and feldspar, which generates stress within the rock's crystalline structure. By 600°C, the quartz phase transition triggers a network of interconnected microcracks, especially in quartz-rich samples (e.g., NB and NZ), significantly altering the rock's structural integrity. A relative increase in P-wave velocity is observed at this temperature due to initial volumetric expansion and reduced porosity. Specifically, PWVD increased from 2.17 to 4.71 km/s in KD, from 2.89 to 4.77 km/s in TB, from 1.86 to 3.84 km/s in NZ, and from 2.71 to 5.12 km/s in NB. Similarly, PWVS rose from 4.26 to 4.9 km/s in KD, 4.49 to 4.75 in TB, 3.30 to 3.84 in NZ, and 4.56 to 5.33 in NB.

At 750°C, the samples show varying thermal responses. The collapse of NB granite highlights its vulnerability to thermal stress, attributed to its larger quartz crystals (100 μm – 3 mm). In contrast, the NZ, KD, and TB samples display wider microcracks and the propagation of trans-crystalline microcracks, indicating significant structural weakening. By 750°C and 900°C, the connectivity of trans-crystalline microcracks becomes dominant, further reducing P-wave velocity and leading to structural degradation. At these temperatures, PWVDs dropped to below 1.3 km/s, and PWVSs fell to less than 2.7 km/s, indicating severe internal damage in the granite samples.

These findings underscore the importance of microstructural characteristics and mineral composition in determining the thermal behavior of granites. Quartz-rich samples, including NZ and NB, are more prone to severe microcracking. In contrast, feldspar and mica minerals facilitate the development of inter-crystalline and trans-crystalline microcracks due to their inherent weaknesses, such as cleavage planes and anisotropic thermal properties.

In practical applications, understanding the thermal sensitivity of granites is essential for predicting their performance under high-temperature conditions, such as in geothermal energy projects, fire-exposed structures, and high-temperature industrial processes. This study provides a novel integrated assessment of thermal effects on microcracks development, porosity, water absorption, and P-wave velocity across four Iranian granites with different geological origins. The innovative use of fluorescence microscopy for quantifying microcracks behavior, along with systematic measurements of physical properties, offers a comprehensive framework for evaluating thermal stability. While most previous studies have investigated

thermal effects on granites up to around 800°C, this research extends microcracks analysis up to 1050°C, providing new insights into high-temperature behavior beyond the commonly studied range. These findings are particularly valuable for enabling the selection of appropriate granite types based on their structural integrity and performance under thermal stress. The research methodology and findings presented in this study can be utilized to examine the behavior of similar granitic rocks under comparable temperature ranges, offering valuable insights into their quality and performance.

Acknowledgment

Tarbiat Modares University financially supported this study. The authors thank Dr. Ahmad Zalooli and Dr. Shahram Ghasemi for their cooperation.

Declaration of Competing Interest

The authors declare that they have no known competing financial interests or personal relationships that could have appeared to influence the work reported in this paper.

Declaration of Generative AI and AI-assisted technologies in the writing process

During the preparation of this work, the author(s) used ChatGPT Openai to improve the readability and language of the paper. After using this tool/service, the author(s) reviewed and edited the content as needed and took (s) full responsibility for the publication's content.

References

Ahmadi, L., Ghobadi, M., Sepahi Garoo, A.A., Izadikian, L., Jafari, S.R., 2023. Evaluating the Effect of Thermal Shock on the Development of Micro-microcracks in Granitoids Using Capillary Water Absorption Test and P-wave velocity Test. Geopersia, 13(1): 103-121. https://doi.org/10.22059/GEOPE.2022.347814.648671

Alcock, T., Bullen, D., Benson, PM., Vinciguerra, S., 2023. Temperature-driven micro-fracturing in granite: The interplay between microstructure, mineralogy and tensile strength. Heliyon 9(3):e13871. https://doi.org/10.1016/j.heliyon.2023.e13871

Berrezueta, E., Kovacs, T., 2017. Application of optical image analysis to the assessment of pore space evolution after CO2 injection in sandstones. A case study. Journal of Petroleum Science and Technology, 159 (Supplement C): 679-690. https://doi.org/10.1016/j.petrol.2017.08.039

Bribiesca Vazquez, S., Mejia Velazquez, J., Reyes Gasga, J., 1998. Alumina additions affect elastic properties of electrical porcelains. American Ceramic Society Bulletin, 77(4):81-85. https://doi.org/10.1088/1755-1315/596/1/012033

Clark, S.P., 1966. Handbook of physical constants. Geological society of America.

Crosby, Z.K., Gullett, P.M., Akers, S.A., Graham, S.S., 2018. Characterization of the mechanical behavior of salem limestone containing thermally-induced microcracks. International Journal of Rock Mechanics and Mining Sciences, 101:54-62. https://doi.org/10.1016/j.ijrmms.2017.11.002

Durham, W. B., Beiriger, J.M., Weed, H.C., 1985. A rapid technique for counting microcracks in rocks. Scanning Electron Microscopy, 1: 133-142.

Ersoy, A., Waller, M.D., 1995. Textural characterization of rocks. Engineering Geology, 136-39: 123 https://doi.org/10.1016/0013-7952(95)00005-Z

Fan, L.F., Gao, J.W., Wu, Z.J., Yang, S.Q., Ma, G.W., 2018. An investigation of thermal effects on micro-properties of granite by X-ray CT technique. Applied Thermal Engineering, 140: 505-519. https://doi.org/10.1016/j.applthermaleng.2018.05.074

Feng, G., Zhu, C., Wang, X., Tang, S., 2023. Thermal effects on prediction accuracy of dense granite mechanical behaviors using modified maximum tangential stress criterion. Journal of Rock Mechanics and Geotechnical Engineering, 15(7):1734-1748.

Feng, Z.J., Zhao, Y.S., Zhang, Y., Wan, Z.J., 2014. Critical temperature of permeability change in thermally cracked granite. Journal of China Coal Society, 39(10): 1987-92.

Fredrich Joanne, T., Teng-fong, W., 1986. Micromechanics of thermally induced cracking in three crustal rocks. Journal of Geophysical Research: Solid Earth, 91.B12: 12743-12764. https://doi.org/10.1029/JB091iB12p12743

Freire-Lista, D.M., Fort, R., Varas-Muriel, M.J., 2016. Thermal stress-induced microcracking in building granite. Engineering Geology, 206: 83-93. https://doi.org/10.1016/j.enggeo.2016.03.005

Gao, H., Lan, Y., Guo, N., 2021. Pore structural features of granite under different temperatures. Materials, 14(21): 6470. https://doi.org/10.3390/ma14216470

Ghasemi, S., Khamehchiyan, M., Taheri, A., Nikudel, M.R., Zalooli, A., 2020. Crack evolution in damage stress thresholds in different minerals of granite rock. Rock Mechanics and Rock Engineering, 53: 1163-1178.

Gomah, M.E., Li, G., Omar, A.A., Abdel Latif, M.L., Sun, C., Xu, J., 2024. Thermal-Induced Microstructure Deterioration of Egyptian Granodiorite and Associated Physico-Mechanical Responses. Materials, 17(6): 1305. https://doi.org/10.3390/ma17061305

Gómez-Heras, M., Gómez Villalba, L.S., Fort González, R., 2010. Cambios de fase en litoarenitas calcáreas con la temperatura: implicaciones para el deterioro causado por incendios. Macla Rev. Soc. Esp. Mineral, pp. 101-102

Hazen, R.M., Finger, L.W., 1982. Comparative crystal chemistry: Temperature, pressure, composition, and the variation of crystal structur,. Chichester: John Wiley & Sons.

Hale, P.A., Shakoor, A., 2003. A laboratory investigation of the effects of cyclic heating and cooling, wetting and drying, and freezing and thawing on the compressive strength of selected sandstones. Environmental and Engineering Geoscience, 9(2): 117-130.

Hall, K.,1999. The role of thermal stress fatigue in the breakdown of rock in cold regions. Geomorphology 31(1-4): 47-63.

Hall, K., Thorn, C.E., 2014. Thermal fatigue and thermal shock in bedrock: An attempt to unravel the geomorphic processes and products. Geomorphology 206: 1-13.

Homand-Etienne, F., Houpert, R., 1989. Thermally induced microcracking in granites: characterization and analysis. International Journal of Rock Mechanics and Mining Sciences & Geomechanics, 26(2): 125-134. Pergamon. https://doi.org/10.1016/0148-9062(89)90001-6

Homand-Etienne, F., Troalen, J.P., 1984. Behaviour of granites and limestones subjected to slow and homogeneous temperature changes. Engineering Geology, 20(3): 219-233. https://doi.org/10.1016/0013-7952(84)90002-4

Huang, Y., Li, T., 2023. On the relationship between the mechanical strength and mineral microstructure of biotite granite under temperature influence. Frontiers in Earth Science, 11: 1209433. http://dx.doi.org/10.3389/feart.2023.1209433

Huang, Y. H., Yang, S. Q., Tian, W. L., Zhao, J., Ma, D., Zhang, C. S., 2017. Physical and mechanical behavior of granite containing pre-existing holes after high temperature treatment. Archives of Civil and Mechanical Engineering, 17(4): 912-925. https://doi.org/10.1016/j.acme.2017.03.007

Isaka, B.A., Ranjith, P.G., Rathnaweera, T.D., Perera, M.S.A., De Silva, V.R.S., 2019. Quantification of thermally-induced microcracks in granite using X-ray CT imaging and analysis. Geothermics, 81: 152-167. https://doi.org/10.1016/j.geothermics.2019.04.007

ISRM, 2007. Rock charactrization, testing and monitoring, ISRM sugested methods. In. Brown ET (ed). Pergamon Press, p211.

Jiang, H., Chen, T., Kang, F., Wang, F., Guo, L., Cao, Y., 2023. Morphological Features of Fractures Developed by Direct Shearing of Intact Granites after Water Cooling Cycles. ACS omega, 8(15): 13639-13648.

Jin, P., Hu, Y., Shao, J., Zhao, G., Zhu, X., Li, C., 2019. Influence of different thermal cycling treatments on the physical, mechanical, and transport properties of granite. Geothermics, 78: 118-128.

Kranz, R.L., 1979. Crack growth and development during creep of Barre granite. International Journal of Rock Mechanics and Mining Sciences, Elsevier, pp 23-35. https://doi.org/10.1016/0148-9062(79)90772-1

Kumari, W.G.P., Ranjith, P.G., Perera, M.S.A., Chen, B.K., Abdulagatov, I.M., 2017. Temperature-dependent mechanical behaviour of Australian Strathbogie granite with different cooling treatments. Engineering Geology, 229: 31-44. http://dx.doi.org/10.1016/j.enggeo.2017.09.012

Lin, W., 2002. Permanent strain of thermal expansion and thermally induced microcracking in Inada granite. Journal of Geophysical Research: Solid Earth, 107(10): 3-16.

Mao, Q., Chen, J., Wu, W., Li, R., Shi, S., Wang, Z., Cui, S., 2023. Multiple Self-Healing Effects of Water-Absorbing Microcapsules in Cementitious Materials. Polymers 15(2): 428.

Mo, C., Zhao, J., Zhang, D., 2022. Real-Time Measurement of Mechanical Behavior of Granite During Heating–Cooling Cycle: A Mineralogical Perspective. Rock Mechanics and Rock Engineering, 55(7): 4403-4422.

Murru, A., Freire-Lista, D.M., Fort, R., Varas-Muriel, M.J., Meloni, P., 2018. Evaluation of post-thermal shock effects in Carrara marble and Santa Caterina di Pittinuri limestone. Construction and Building Materials, 186: 1200-1211.

Pan, J., Xi, X., Wu, X., Guo, Q., Ren, F., Cai, M., 2023. Physical properties evolution and microscopic mechanisms of granite modified by thermal and chemical stimulation. Case Studies in Thermal Engineering, 41: 102633. https://doi.org/10.1016/j.csite.2022.102633.

Philpotts, A.R., Ague, J.J., 2009. Principles of igneous and metamorphic petrology. Cambridge University Press.

Ruzyla, K., 1986. Characterization of pore space by quantitative image analysis. SPE Formation Evaluation, 1.04: 389-398.

Samouh, H., Ishikawa, S., Kontani, O., Murakami, K., Nishimoto, S., Suzuki, K., Maruyama, I., 2021. Thermomechanical behavior of granite under 150° C: experimental and numerical analysis. Materials and Structures, 54: 1-16. https://doi.org/10.1617/s11527-021-01830-7.

Shao, S., Wasantha, P.L.P., Ranjith, P.G., Chen, B.K., 2014. Effect of cooling rate on the mechanical behavior of heated Strathbogie granite with different grain sizes. International Journal of Rock Mechanics and Mining Sciences, 70: 381-387. http://dx.doi.org/10.1016/j.ijrmms.2014.04.003

Shen, Y., Hou, X., Yuan, J., Xu, Z., Hao, J., Gu, L., Liu, Z., 2020. Thermal deterioration of high-temperature granite after cooling shock: multiple-identification and damage mechanism. Bulletin of Engineering Geology and the Environment, 79: 5385-5398.

Shen, Y., Yuan, J., Hou, X., Hao, J., Bai, Z., Li, T., 2021. The strength changes and failure modes of high-temperature granite subjected to cooling shocks. Geomechanics and Geophysics for Geo-Energy and Geo-Resources, 7: 1-18.

Shi, X., Gao, L., Wu, J., Zhu, C., Chen, S., Zhuo, X., 2020. Effects of cyclic heating and water cooling on the physical characteristics of granite. Energies, 13(9): 2136.

Skinner, B.J., 1966. Section 6: Thermal Expansion. In: Clark SP, Jr. (ed) Handbook of Physical Constants, Geological Society of America Bulletin, http://dx.doi.org/10.1016/0022-4596(73)90118-7

Somerton, W.H., 1992. Chapter IV. Thermal Expansion of Rocks. In: Somerton WH (ed) Developments in Petroleum Science. Elsevier, pp 29-38. http://dx.doi.org/10.1007/978-3-642-34023-9_2

Sousa, L.M., del Río, L.M.S., Calleja, L., de Argandona, V.G.R., Rey, A.R., 2005. Influence of microfractures and porosity on the physico-mechanical properties and weathering of ornamental granites. Engineering Geology, 77(1-2): 153-168.

Štubňa, I., Trník, A., Vozár, L., 2007. Thermomechanical analysis of quartz porcelain in temperature cycles. Ceramics International, 33(7): 1287-1291.

Taylor, D., 1972. The thermal expansion behaviour of the framework silicates. Mineralogical Magazine 38.297: 593-604.

Tronskar, J.P., Mannan, M.A., Lai, M.O., 2003. Application of acoustic emission for measuring crack initiation toughness in instrumented Charpy impact testing. Journal of Testing and Evaluation, 31(3): 222-233.

Vázquez, P., Alonso, F., Esbert, R., Ordaz, J., 2010. Ornamental granites: Relationships between p-waves velocity, water capillary absorption and the crack network. Construction and Building Materials, 24(12): 2536-2541.

Vázquez, P., Shushakova, V., Gómez-Heras, M., 2015. Influence of mineralogy on granite decay induced by temperature increase: Experimental observations and stress simulation. Engineering Geology, 189: 58-67.

Van der Molen I., 1981. The shift of the α-β transition temperature of quartz is associated with the thermal expansion of granite at high pressure. Tectonophysics, 73(4): 323-342.

Wang, L.C. and Bao, J., 2019. Experimental Investigation on Capillary Water Absorption in Discrete Planar Crack. JTRPROGRAM. http://dx.doi.org/10.1016/j.conbuildmat. 2017.04.129

William, H., Turner, F., Gilbert, C.M., 1954. Petrography, An Introduction to the Study of Rocks in Thin Section. University of California, Berkeley, WH Freeman and Company.

Wu, Q., Weng, L., Zhao, Y., Guo, B., Luo, T., 2019. On the tensile mechanical characteristics of fine-grained granite after heating/cooling treatments with different cooling rates. Engineering Geology, 253: 94-110. http://dx.doi.org/10.1016/j.enggeo.2019.03.014

Yang, S.Q., Ranjith, P.G., Jing, H.W., Tian, W.L. and Ju, Y., 2017. An experimental investigation on thermal damage and failure mechanical behavior of granite after exposure to different high temperature treatments. Geothermics, 65: 180-197.

Yang, S.Q., Tian, W.L., Elsworth, D., Wang, J.G. and Fan, L.F., 2020. An experimental study of the effect of high temperature on the permeability evolution and failure response of granite under triaxial compression. Rock Mechanics and Rock Engineering, 53: 4403-4427.

Yavuz, H., Demirdag, S., Caran, S., 2010. Thermal effect on the physical properties of carbonate rocks. International Journal of Rock Mechanics and Mining Sciences, 47(1): 94-103.

Yin, T.b., Shu, R.h., Li, X.b., Wang, P., Liu, X.l., 2016. Comparison of mechanical properties in high temperature and thermal treatment granite. Transactions of Nonferrous Metals Society of China 26(7): 1926-1937.

Yin. T., Bai, L., Li, X., Li, X., Zhang, S., 2018. Effect of thermal treatment on the mode I fracture toughness of granite under dynamic and static coupling load. Engineering Fracture Mechanics, 199: 143-158.

Zalooli, A., Khamehchiyan, M., Nikudel, M. R., Freire-Lista, D. M., Fort, R., Ghasemi, S., 2020. Artificial microcracking of granites subjected to salt crystallization aging test. Bulletin of Engineering Geology and the Environment, 79: 5499-5515.

Zhao, J., Sun, W., Luo, H., Wu, S., Hou, Z., 2024. Effect of thermal treatment on microcracking characteristics of granite under tensile condition based on bonded-particle model and moment tensor. Scientific Reports, 14(1): 8806. https://doi.org/10.1038/s41598-024-59470-0

Zhang, K., Cheng, Y., Li, W., Hao, C., Hu, B., Jiang, J., 2019. Microcrystalline characterization and morphological structure of tectonic anthracite using XRD, liquid nitrogen adsorption, mercury porosimetry, and micro-CT. Energy and Fuels, 33(11): 10844-10851.

Zhang, W., Sun, Q., Zhang, Y., Xue, L., Kong, F., 2018. Porosity and wave velocity evolution of granite after high-temperature treatment: a review. Environmental Earth Sciences, 77: 1-13.
https://doi.org/10.1007/s12665-018-7514-3

Zuo, J.P., Wang, X.S., Mao, D.Q., Wang, C.L., Jiang, G.h., 2016. effects of T–M coupled on cracking behaviors and reliability analysis of double-notched crustal rocks. Engineering Fracture Mechanics, 158: 106-115. http://dx.doi.org/10.1016/j.engfracmech.2015.11.001